Scientific Journals
Scientific Journal of Review (2016) 5(3) 360-370
ISSN 2322-2433
doi: 10.14196/sjr.v5i3.2137

Contents lists available at Sjournals
Scientific Journal of **Review**
Journal homepage: www.Sjournals.com

Original article

The effect of nickel doping on the structural, defect structural, optical and magnetic properties of zinc oxide nanoparticles

Mona Mohsen[a], Mohammed Mohammed El Okr[b], Ehsan Gomaa[a,*], Emad Hassan Ali[a], Mohammed Essam[c]

[a]*Physics Department Faculty of Science, Ain Shams University, Cairo, Egypt.*
[b]*Physics Department, Faculty of Science, Al Azhar University, Cairo, Egypt.*
[c]*Physics Department Faculty of Engineering, Modern Academy, Cairo, Egypt.*

*Corresponding author; Physics Department Faculty of Science, Ain Shams University, Cairo, Egypt.

ARTICLE INFO

Article history,
Received 19 February 2016
Accepted 18 March 2016
Available online 25 March 2016
iThenticate screening 22 February 2016
English editing 15 March 2016
Quality control 21 March 2016

Keywords,
Zinc oxide
PALS
Magnetization
Nanoparticles
Energy gap

ABSTRACT

Positron annihilation lifetime (PAL) spectroscopy has been applied in the present work to study the defect structure changes of the $Zn_{1-x}Ni_xO$ ($0\% \le x \le 10\%$). This system has been synthesized in nanosize by coprecipitation method. Nanostructure features of the prepared samples have been investigated by X-Ray diffraction (XRD) and TEM. The XRD data has revealed that the prepared samples are crystalline and belong to space group $P6_3mc$. The deduced estimated average crystallite size is varying from 20 nm to 96 nm in agreement with TEM measurements The variation of lattice parameters and internal strain that have been deduced from XRD data, have shown that the solubility limit of NiO in ZnO does not exceed 5% and are correlated with PAL parameters. At 7% and 10% concentrations the XRD spectra has revealed the presence of secondary peaks due to creation of a new NiO phase, which indicates that Ni is no more incorporated in the ZnO structure. This has been also confirmed by the variation of the energy gap E_g deduced from the UV absorbance spectra and the variation of FTIR absorption bands. The (M-H) curves have shown that the saturation magnetization M_s suggest the presence of ferromagnetism which decreases with increasing Ni content up to 5%. This is associated with an increase in the formation of vacancy clusters and positron trapping rate in the

interface region. In addition, the vacancy defects play an important role in mediating the ferromagnetism behavior in agreement with the polaron model.

1. Introduction

Nanocrystalline materials are single or multi-phase polycrystalline solids with a grain size of a few nanometers (1 nm = 10^{-9} m = 10 Å), typically less than 100 nm. Materials having grain size of ~ 0.1 to 0.3 μm are classified as submicron materials. Nanocrystalline materials are composed of interfaces, mainly grain boundaries. Consequently, nanocrystalline materials exhibit properties that are significantly different from their conventional coarse-grained polycrystalline counterparts. Materials with microstructural features of nanometric dimensions are referred in the literature as nanocrystalline materials (a very generic term). Microstructural features on a nanometer-scale have been known to be useful in enhancing the properties and performance of materials. Diluted magnetic semiconductors (DMS) have attracted a wide attention due to their unique properties and immense potential applications such as spintronics (Das Sarma, 2001), transparent electronics, ultraviolet (UV) light emitters, piezoelectric devices, chemical sensors and heterogeneous photocalysts (Das Sarma, 2001; Matsumoto et al., 2001).

Zinc oxide (ZnO) is an n-type semiconductor and has a direct wide band gap (3.4 eV at room temperature). In ambient condition, ZnO has a stable hexagonal wurtzite structure with lattice spacing a = 0.325 nm and c = 0.521 nm and is composed of a number of alternating planes with tetrahedrally-coordinated O^{2-} and Zn^{2+} ions, stacked alternately along the c-axis. Magnetic characteristics and potential mechanisms have been widely studied theoretically and experimentally in ZnO doped with transitional metals (Dietl et al., 2000; Katayama-Yoshida et al., 2007). As one of the best candidates, ZnO is a direct band gap semiconductor with a hexagonal (Wurtzite) crystal structure. Mohapatra et al (2011) as well as Teodora et al (2012) used the solid state reaction and sol gel reaction respectively to study the structural and magnetic properties of several concentrations of Ni doped ZnO. On the other hand, Chauhan et al (2012) investigated the structural and optical properties of different concentrations of Ni doped ZnO nanocrystals.

In the present work, Ni doped ZnO nanoparticles of concentrations (0%, 1%, 3%, 5%, 7%, 10%) have been synthesized by using chemical coprecipitation method. Transmission electron microscope (TEM), XRD are applied for microstructure identification. Ultraviolet (UV), Fourier Transform Infrared (FTIR) and magnetic hysteresis have been applied to investigate the optical and magnetic properties respectively. Coprecipitation method is a promising method because of the low cost and process temperature as well as the easy way to control the particle size. Some of the most commonly substances used in coprecipitation operations are hydroxides, carbonates, sulphates and oxalates. Various chemical methods have been also developed to prepare ZnO nanocrystals such as sol-gel synthesis (Park and Kim, 2003), hydrothermal and solid state reactions. Zhi-Yuan Chen et al (2012) investigated the effect of defects on the magnetic properties of Ni-doped ZnO nanocrystals, which are prepared by solid state reaction, using positron annihilation technique. The authors suggested that the ferromagnetism in Ni-doped ZnO with 4% and 20% is probably mediated by vacancy defects in the interface region in the frame work of polaron model (Tian et al., 2011). The relationship between the microstructure and optical as well as magnetic properties is established with the aim to clarify the origin of observed room temperature ferromagnetism (RTFM) whether intrinsic or extrinsic as well as the effect of open volume defects using positron annihilation lifetime technique. In the intrinsic case the RTFM will arise from Ni ion substitution in Zn sites whereas in the extrinsic case it will be due to formation of Ni-Ni clusters (Ankiewicz et al., 2010).

2. Materials and methods

2.1. Preparation of samples

The $Zn_{1-x}Ni_xO$ (x=0 %, 1%, 3%, 5%, 7%, 10%) series of polycrystalline samples were prepared using $ZnCl_2$ and $NiCl_2$ as starting materials. The stoichiometric amounts of starting chemical materials required for each

composition were mixed thoroughly and calcinated at 600 ^{o}C for 6 hours following several cycles of quenching and grinding. The obtained powders are pressed into pellets of 5 gram by weight and 10 mm diameter with thickness 0.5cm at a pressure of 4 tons / cm^2. The reaction can be demonstrated as follow:

$$(ZnCl_2.6H_2O)_{1-x} + (NiCl_2.6H_2O)_x \rightarrow 2NaOH + Zn_{1-x}Ni_x(OH)_2 + 2NaCl + 6H_2O$$
$$Zn_{1-x}Ni_x(OH)_2 \xrightarrow{heat} Zn_{1-x}Ni_xO$$

Where X= 0%, 1%, 3%, 5%, 7%, 10%.

2.2. Techniques

2.2.1. Transmission electron microscope (TEM)

To ensure that the prepared samples are in nano-form, all of prepared samples are measured by JEL: 1200EX II, Japan. Transmission electron microscope by suspension method; A suspension of sample powder in a solution which is not soluble in it, i.e.: distilled water, is obtained then the grid is dipped in that solution to catch some nano-particles, which will be subjected to the electron beam.

2.2.2. X-Ray diffraction (XRD)

To study the crystalline nature for all prepared samples, the samples were examined by X-ray diffraction using Phillip's computerized diffractometer (type: XPERT-MPDUC PW 3040) equipped with a Cu X-ray tube with CuKα radiation source (λ= 0.15406 nm), at a power of 1600W (40 kV and 40 mA). The particle size is calculated using Scherrer equation (Langford and Wilson, 1978).

2.2.3. UV-visible spectra (UV-Vis)

UV-visible spectra are measured using Jasco V-560 UV-VIS Spectrophotometer.

2.2.4. Fourier transform infrared (FTIR)

In order to get information about the vibrational modes, the FTIR absorption spectra in the region (400 – 4000 cm^{-1}) have been measured using Thermo scientific NICOLET 6700 FTIR, using KBr pellet technique.

2.2.5. Magnetic hysteresis

(M-H) curves are measured for all prepared samples using the vibrating sample magnetometer, VSM, EG & GPARC model 1551, USA.

2.2.6. Positron annihilation lifetime (PAL)

A fast-fast coincidence spectrometer was used for measuring PAL spectra. A 20 μCi source of ^{22}NaCl deposited on a thin Kapton foil (7 m) was sandwiched between two identical specimens. The time resolution full-width at half-maximum (FWHM) of 230 ps. The positron lifetime spectra were recorded at RT, more than one million counts were accumulated. The lifetime spectra were analyzed into two components using the LT 9.0 program (Kansy, 2001). The component characterized by the short lifetime τ_1 with intensity I_1 represents the positron annihilating in the monovacancies and dislocations. The long lifetime τ_2 with intensity I_2 corresponds for positrons trapped and annihilating in three-dimensional vacancies and vacancy clusters. From the data analysis of positron experiment, the trapping rate κ of positron were deduced on the basis of the two state trapping mode (Hautojarvi and Corbel, 1995).

3. Results and discussion

3.1. Transmission electron microscopy

The TEM pictures of Ni-doped ZnO are shown in Fig. 1 (a –f). Fig. 1 shows that all the prepared samples are in nano-form and there is a variation in 1% Ni doped ZnO, where the grains are identical in shape. But in 3% Ni-doped ZnO, the grains are well connected with less intergranular spacing. At higher Ni concentration the intergrain connectivity decreases and the intergranular spacing increases due to the formation of NiO clusters. Some previous work (Egerton et al., 2004), showed that the electron beam in TEM has a damage effect with increasing

the electron dose on sample. This damage may include heating, electrostatic charging, ionization damage, displacement damage, sputtering, and hydrocarbon contamination. This may be a reason for the agglomeration that occurred in Fig. 1 (f) at 10% Ni concentration.

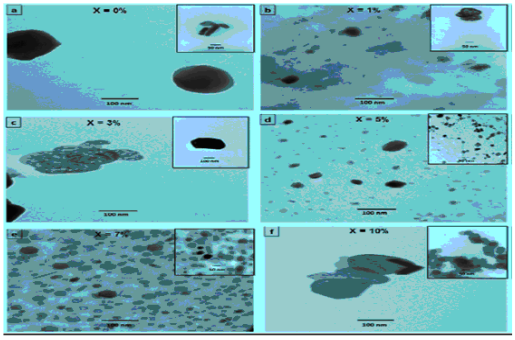

Fig. 1 (a – f). TEM for Zn(1-X)Ni(X)O: a) for pure Zinc Oxide, b) for 1% of NiO, c) for 3% NiO, d) for 5% NiO, e) for 7% of NiO, and f) for 10% NiO.

3.2. X-Ray diffraction spectra

XRD diffraction spectra are measured for all prepared samples of $Zn_{(1-X)}Ni_{(X)}O$ and are shown in Fig. 2. All the samples are polycrystalline in nature having all the peaks corresponding to wurtzite structure of ZnO. A weak secondary phase of NiO was observed in low concentration of Ni-doped samples. The peak intensity of NiO increases with the increase of Ni concentration. It is very well known that Zn has an atomic radius of 0.74 Å and forms a stable oxidation state of 2. However, Ni has an atomic radius of 0.69 Å and is very much unstable in the ZnO matrix. So, it has the tendency to form clusters of metallic Ni or NiO especially at higher concentration (>5%) this is indicated in the XRD pattern by the presence of the 2 lines of NiO at x = 7% and 10% as shown in Fig. 3. Hence, the presence of NiO is evidenced in the XRD pattern, which suggests that Ni in higher percentage (>5%) does not incorporate in the ZnO matrix and forms secondary phases like NiO, which indicates the achievement of the limit of solubility.

By using Scherrer equation particle size is calculated and plotted as a function of nickel content as shown in Fig. 4. It is clear that particle size varies from 20.7 nm in pure zinc oxide till it reaches 95.3 nm at 7% nickel concentration then remains constant. Lattice parameters a and c are calculated for all concentrations and plotted in Fig. 5. A monotonic variation occurs in the lattice parameters till 5% nickel concentration then weak variation is observed at 7% and 10% thus suggesting solubility limit. By using Williamson Hull plot, the internal strain has been deduced for each concentration from the slope of the straight line. Fig. 6 shows the plot for 5% doped sample as an example. The variation of the deduced internal strain with Ni content is shown in Fig. 7. It is observed that, the internal strain increases till 5% Ni concentration then starts to decrease this may be an indication for reaching the solubility limit.

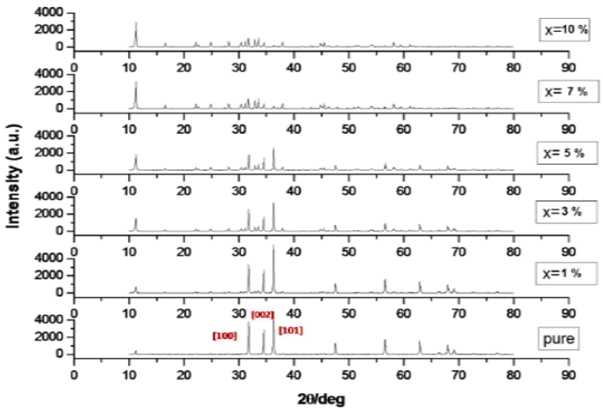

Fig. 2. XRD pattern for all concentrations.

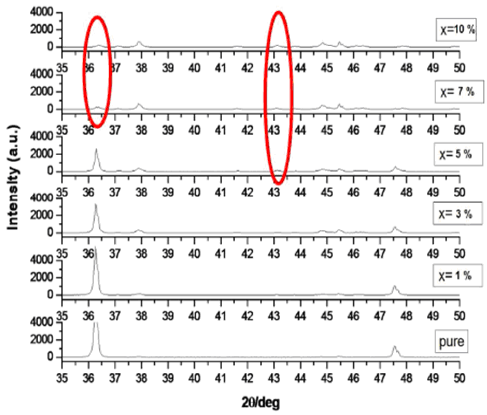

Fig. 3. Occurrence of Ni peaks after 5% Ni concentration.

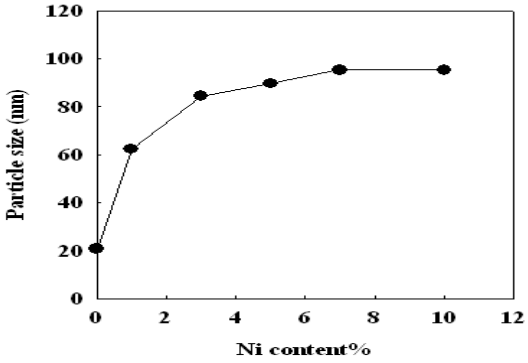

Fig. 4. Variation of particle size with Nickel content.

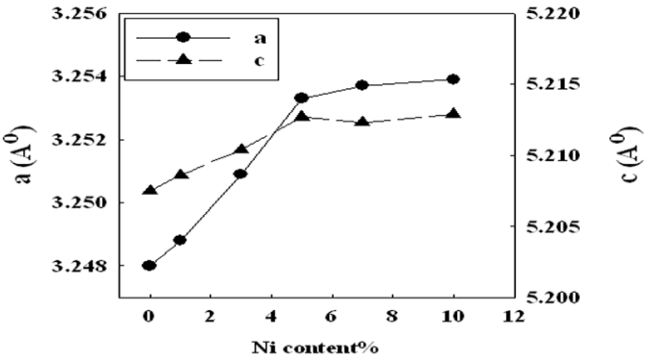

Fig. 5. Variation of lattice parameters a, c with Nickel content.

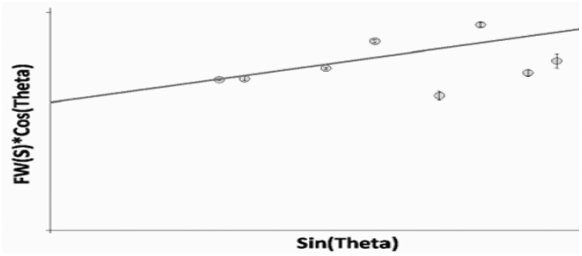

Fig. 6. Williamson Hull plot for the 5% doped sample as an example.

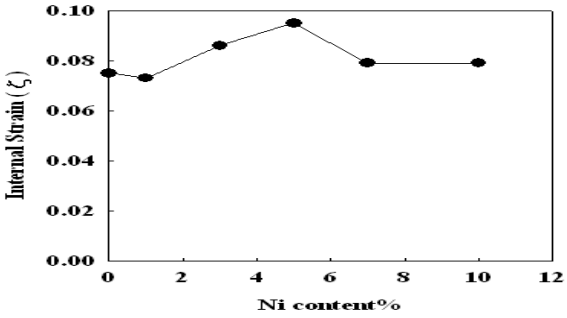

Fig. 7. Variation of internal strain with nickel content.

3.3. UV-visible spectroscopy

The absorbance of UV-Visible spectra for all concentrations is shown in Fig. 8. Tauc relation is used to make the plot of Fig. 9 to get values of the energy gap which is performed by a linear fitting at the straight portion of curve. Fig. 10 demonstrates the variation of the energy gap E_g with Ni content. Before 5% Ni concentration E_g decreases with increasing Ni concentration (peaks red shifted). At higher concentrations E_g increases (peaks blue shifted) thus indicating that no more doping can occur (solubility limit), which is in agreement with X-ray results.

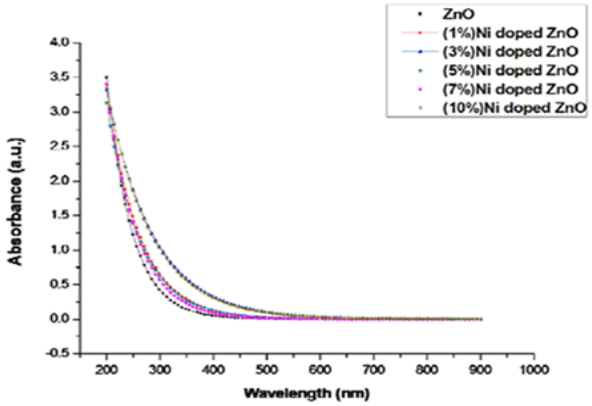

Fig. 8. Absorbance of UV-Vis spectrum for all concentrations.

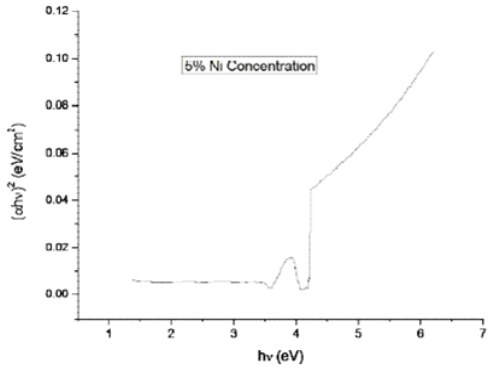

Fig. 9. Tauc plot at 5% Ni concentration as an example.

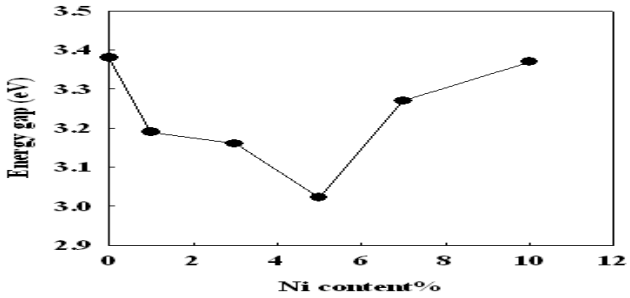

Fig. 10. Variation of energy gap with Ni content.

3.4. Fourier transform infrared analysis

The FTIR spectrum has shown medium, weak, and broad absorption bands. Hence the effect of composition on various types of structural units within each series is not much significant. The finger print infrared absorption peaks of zinc oxide network vibrational modes are present in all samples. Fig. 11 shows the IR absorbance peaks for all samples and indicate the band positions and their corresponding assignments. Water and carbon dioxide modes occur due to the preparation of samples in open air. Also blue shift occurs for the peak at 900 cm^{-1} after 5% Ni concentration, which indicates no more incorporation of Ni inside ZnO lattice, thus giving the signal of a solubility limit in accordance with X-ray and UV results.

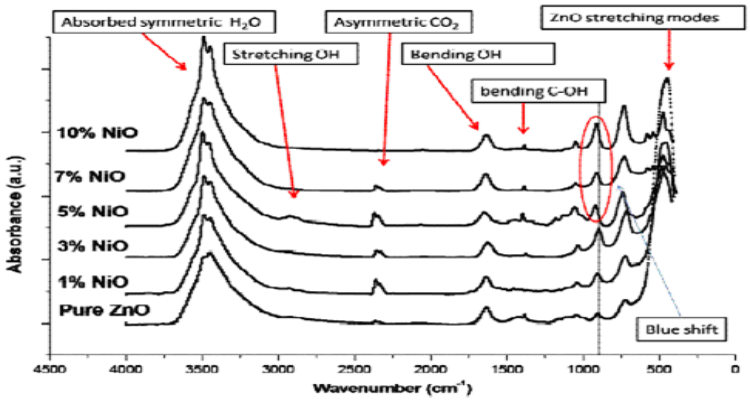

Fig. 11. FTIR spectra of Zn(1-X)Ni(X)O for different Ni concentrations.

3.5. Magnetic hysteresis measurements

(M-H) curves are measured at room temperature for all samples and are shown in Fig. 12. It is to be noted that the saturation magnetization M_s of non doped ZnO and Ni-doped samples show room temperature ferromagnetism (RTFM). Saturation magnetization (M_s) value is deduced from the curves. The variation of M_s with Ni content is shown in Fig. 13. According to Rudderman–Kittel–Kasuya–Yoshida (RKKY) theory (Stephen and Ferrira, 2013), the magnetism i.e. the spin polarization is due to the p-d exchange interaction between O 2p and Ni 3d orbitals. M_s decreases with Ni concentrations reaching a minimum at 5% and 7% signaling the solubility limit, where Ni is not anymore incorporated inside ZnO lattice. This confirms the fact that, the origin of RTFM is intrinsic i.e. due to the substitution of Zn with Ni. Furthermore, it shows that Ni doping quenches the exchange interaction and consequently the ferromagnetism. The correlation of M_s with vacancy defect will be investigated in the next section dealing with PAL results.

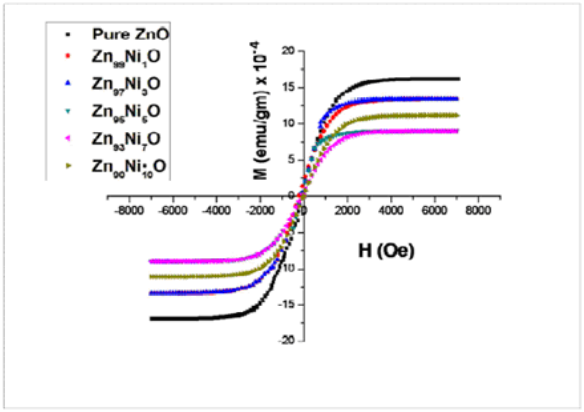

Fig. 12. Magnetic hysteresis for all samples at room temperature.

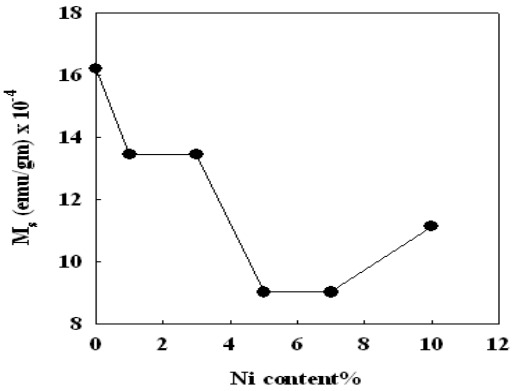

Fig. 13. Saturation magnetization variation with concentration.

3.6. Positron annihilation lifetime

The analysis of positron annihilation spectra could be fitted with two lifetime components indicating the annihilation of positrons at two sites. τ_1 and I_1 are related to lifetime and intensity of free annihilation of positrons in the crystal interstitial sites *(*Fig. 14*),* whereas τ_2 and I_2 give the lifetime and intensity for the annihilation of trapped positrons in open volume defects (vacancies, voids or grain boundaries) as shown in Fig. 15.

At Ni-concentration x = 1%, τ_1 decreases from 0.2 ns to 0.09 ns, indicating a reduction in the size of interstitial sites, which can be due to the incorporation of Ni interstitially. This is in accordance with XRD spectrum at x = 1%, where no change in the relative intensities of the ZnO peaks is observed, thus revealing no incorporation of Ni into the ZnO lattice. At higher Ni concentrations, τ_1 increases and the probability of free annihilation I_1 reaches 94% up to 5% Ni content. This can be explained by the increase in the lattice parameters due to the substitution of Zn^{+2} by Ni^{+2} with smaller Ni radius of 0.69 Å compared to Zn radius of 0.7Å. This is evidenced by a positive correlation of τ_1 and a as well as c lattice parameters as shown in Figs. (16, 17). At 7% and 10% concentrations the probability of free annihilation I_1 decreases to 81% and the probability of positrons trapped at open volume defects I_2 increases by almost 3 times (I_2 increases from 5% at low Ni concentrations to an average of 15% at 7% and 10% Ni concentrations. τ_2 reaches a maximum of 1ns at 5% Ni content and is found to be positively correlated with the variation of the internal strain (Fig. 18) showing also a maximum at 5% Ni concentration. At the latter concentration M_s decreases to reach half its value, which indicates that the suppression of RTFM can be mediated by factors such as strain and open volume defects (Fig. 19). This behavior can be explained on the basis of the magnetic polaron model (Chou et al., 2010; Kaminski and Das Sarma, 2002). According to this model, vacancy defect induced ferromagnetism can arise through binding the spins of magnetic ions to form bound magnetic polarons (BMPs), which has experimentally confirmed recently by several authors (Pandey et al., 2010; Abdel Hakeem, 2010).

In order to determine the nature of vacancies from τ_2, the ratio of τ_2 to the bulk lifetime, which has been measured (Chen et al., 2003) for ZnO single crystal to be in the range between 170-181 ps is used. Our measured free annihilation lifetime τ_1 varies from 85 ps to 170 ps with Ni content. Using τ_1 = 170 ps at 5% the ratio is determined to be 5.88 indicating the formation of big vacancy agglomerates at the solubility limit. Therefore one can conclude that, the decrease in M_s is due to a reduction in the ferromagnetic coupling induced by the formation of vacancy clusters (oxygen vacancies) at the interface region in agreement with (Mohapatra et al., 2011; Chen et al., 2012). Fig. 20, also shows the trapping rate κ as a function of Ni content, showing a minimum at 3% and 5% Ni concentration and maximum at 7% concentration thus indicating increase in defects concentration from $15x10^{17}$ cm^{-3} to $85x10^{17}$ cm^{-3}. Fig. 20 also shows that κ is positively correlated with the variation of E_g. The decrease in the energy gap indicates that Ni is incorporated in the ZnO lattice leading to a smaller trapping rate of positrons at the solubility limit.

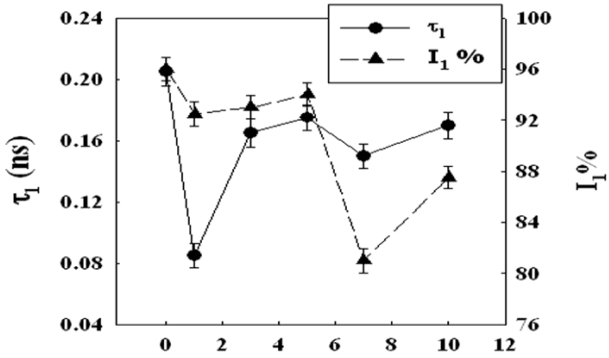

Fig. 14. Variation of free annihilation lifetime τ_1 and its intensity I_1 with Ni content.

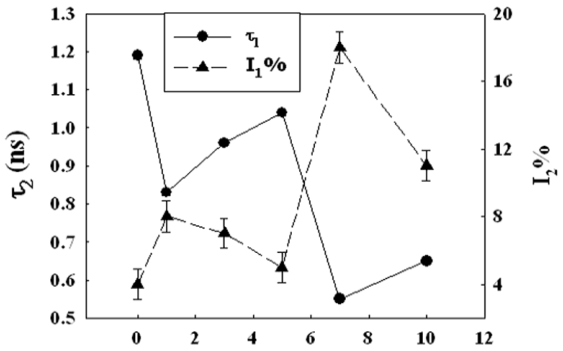

Fig. 15. Variation of defect lifetime τ_2 and its intensity I_2 with Ni content.

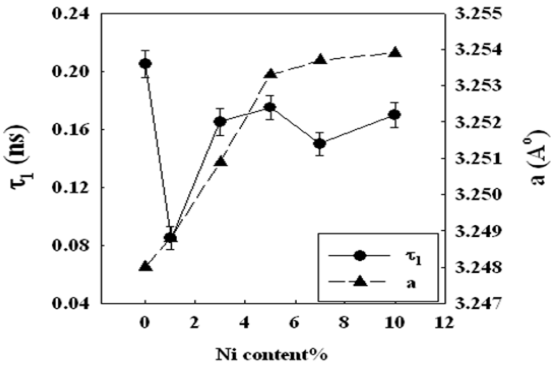

Fig. 16. Variation of bulk lifetime and lattice parameter a.

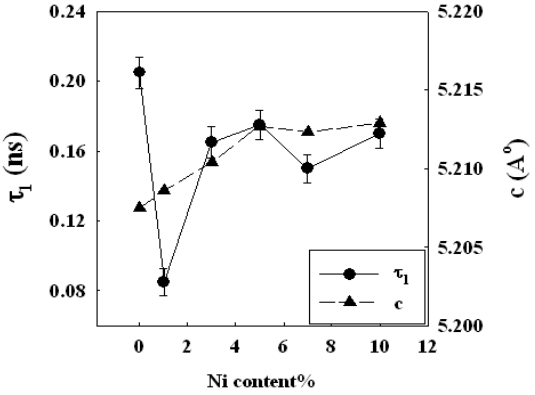

Fig. 17. Variation of bulk lifetime and lattice parameter c.

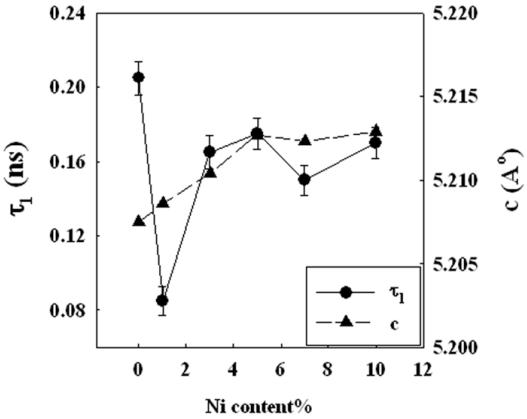

Fig. 18. Variation of defect lifetime and internal strain.

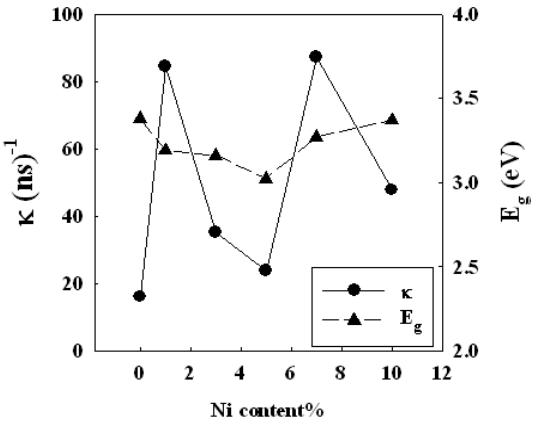

Fig. 19. Variation of τ_2 and M_s with Ni concentration.

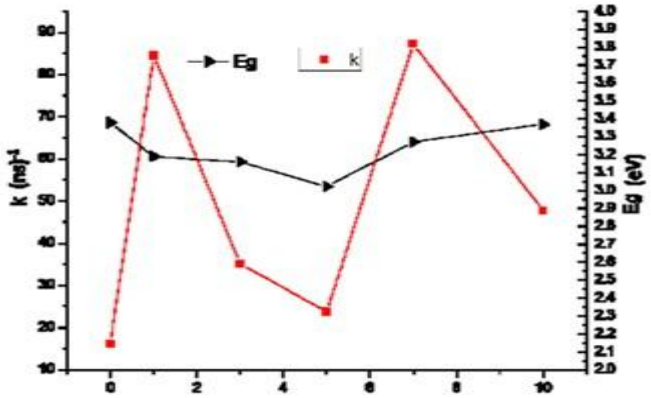

Fig. 20. Variation of trapping rate and energy gap.

4. Conclusion

* NiO doped ZnO nanocrystals with concentrations (1%, 3%, 5%, 7% and 10%), have been prepared by coprecipitation method.
* XRD patterns revealed that the samples are polycrystalline with all the peaks corresponding to wurtzite structure of ZnO, with the presence of a NiO secondary phase at high Ni concentrations.
* From XRD data the average crystallite size is found to increase with Ni concentration from 62 nm to 96 nm. The variation of lattice parameters and internal strain with Ni content which are found to be positively correlated with the variations of the annihilation parameters and, respectively, suggest that 5% is the solubility limit of NiO into ZnO.
* The results are also confirmed by TEM pictures, which show a decrease in intergranular spacing at 7% and 10% Ni content due to the formation of Ni clusters, in accordance with UV and FTIR measurements.
* The saturation magnetization values suggest the presence of ferromagnetism, which decreases with NiO concentration and is found to be associated with an increase in the strain as well as the size of vacancy clusters.
* PAL results confirm the fact, that formation of vacancy clusters in the grains interface can suppress the ferromagnetism in accordance with the polaron model through indirect interactions between bound magnetic polarons mediated by open volume defects.

References

Abdel Hakeem, A.M., 2010. Room –temperature ferromagnetism in Zn1-x Mnx O, J. Magn. Magn. Mater., 322, 709.

Ankiewicz, A.O., Martins, J.S., Carmo, M.C., 2010. Ferromagnetic resonance on metal nanocrystals in Fe and Ni implanted ZnO, J. Appl. Phys., 107, 09B518 -3.

Behan, A.J., Mokhtari, A., Blythe, H.J., 2008. Two magnetic regimes in doped ZnO corresponding to a dilute magnetic semiconductor and a dilute magnetic insulator, Phys. Rev. Lett., 100, 047206.

Chauhan, R., Kumar, A., Chaudhary, R., 2011. Structures and optical properties of Zn 1-x Nix O nanoparticles by co-precipitation method, J. Optoelectron. Biomed. Mater., 3(1), 17-23.

Chen, Z.Q., Yamanoto, S., Maekawa, M., 2003. Postgrowth annealing of defects in ZnO studied by positron annihilation, x-ray diffraction, Rutherford backscattering, cathodoliuminesence, and Hall measurements, J. Appl. Phys., 94, 4807.

Chou, H., Lon, C.P., Hsu, H.S., Sun, S.J., 2010. The role of carries in spin current and magnetic coupling for ZnO: Co diluted magnetic oxides, Appl. Phys. Lett., 96, 092503.

Das Sarma, S., 2001. A new class of device based on electron spin, rather than on charge, may yield the next generation of microelectonics, Am. Sci., 89, 516.

Dietl, T., Ohno, H., Matsukura, F., 2000. Zener model description of ferromagnetism in zinc-blende magnetic semiconductors, Sci., 287, 1019-22.

Egerton, R.F., Li, P., Malac, M., 2004. Radiation damage in the TEM and SEM, Micron 35, 399-409.

Gao, D.Q., Zhang, Z.H., Fu, J.L., 2009. Room temperature ferromagnetism of pure ZnO nanoparticles, J. Appl. Phys., 105(11), 113928-113928-4.

Hautojarvi, P., Corbel, C., 1995. Positron spectroscopy of solids, edited by Dupasquier A and Mills AP, 1st ed North Holland, Amsterdam.

Janisch, R., Gopal, P., Spaldin, N.A., 2005. Transition metal-doped TiO_2 and ZnO-present status of the field, J. Phys. Condens. Matter., 17, 657.

Kaminski, A., Das Sarma, S., 2002. Polaron percolation in diluted magnetic semiconductors, Phys. Rev. Lett., 88, 247202.

Kansy, J., 2001. Positron for positron lifetime analysis adjusted to the PC windows environment, Mater. Sci. Forum., 652, 363-365.

Katayama-Yoshida, H., Sato, K., Fukushima, T., 2007. Theory of ferromagnetic semiconductors, Phys Status Solidi A., 204, 15 – 32.

Kim, D., Yang, J.H., Hong, J., 2009. Ferromagnetism induced by Zn vacancy defect al lattice distortion in ZnO, J. Appl. Phys., 106, 013908.

Langford, J.I., Wilson, A.J.C., 1978. Scherrer after sixty years: A survey and some new results in the determination of crystallite size, J. Appl. Cryst., 11, 102-113.

Liu, C., Yun, F., Moroc, H., 2005. Ferromagnetism of ZnO and GaN: A review, J. Mater. Sci., 16, 555-597.

Malaeru, T., Neamtu, J., Morari, C., Sbacea, G., 2012. Structural and magnetic properties of nanocrystalline powders of Ni-doped ZnO diluted magnetic semiconductors synthesized by sol-gel method, Rev. Roum. Chim., 57(9-10), 857-862.

Matsumoto, Y., Murakami, M., Shono, T., 2001. Room temperature ferromagnetism in transparent transition metal doped titanium dioxide, Sci., 291, 854.

Mohapatra, J., Mishra, D.K., Kamilla, S.K., 2011. Ni- doped ZnO: Studies on structural and magnetic properties, Phys. Status. Solidi., B248(6), 1352-1359.

Ohno, H., 1998. Making nonmagnetic semiconductors ferromagnetic, Sci., 281, 951.

Pandey, B., Ghosh, S., Srivastava, P., 2010. Room temperature transparent ferromagnetism in 200 keV Ni^{2+} ion implanted pulsed laser deposition grown ZnO/sapphire film, J. Appl. Phys., 107, 023901.

Park, Y.R., Kim, K.J., 2003. Sol-gel preparation and optical characterization of NiO and $Ni_{1-x}Zn_xO$ thin films, J. Cryst. Growth., 258, 380-384.

Pearton, S.J., Norton, D.P., Lp, K., 2004. Recent advances in processing of ZnO, J. Vac. Sci. Technol., B 22, 932.

Sato, K., Katayama-Yoshida, H., 2000. Ferromagnetism in a transition metal atom doped ZnO, Physica E., 10(1-3), 251- 255.

Sharma, P.K., Dutta, R.K., Pandey, A.C., 2009. Effect of iron doping concentration on magnetic properties of ZnO nanoparticles, J. Magn. Magn. Mater., 321, 2587-2591.

Stephen, R., Mauro S Ferrira, 2013. Indirect exchange and Ruderman-Kittel-Kasuya- Yosida (RKKY) interactions in Magnetically-doped grapheme, Crystals 3, 49-78.

Tian, Y., Li, Y., He, M., 2011. Bound magnetic polarons and p-d exchange interaction in ferromagnetic insulating Cu-doped ZnO, Appl. Phys. Lett., 98, 162503.

Wang, D., Chen, Z.Q., Wang, D.D., 2010. Positron annihilation study of the interfacial defects in ZnO nanocrystals: Correlation with ferromagnetism, J. Appl. Phys., 107, 023524.

Yan, W.S., Sun, Z.H., Liu, Q.H., 2007. Zn vacancy induced room-temperaure ferromagnetism in Mn-doped ZnO, Appl. Phys. Lett., 91(6), 062113.

Zhi-Yuan Chen, Chen ZQ, Zou B, 2012. Defect mediated ferromagnetism in Ni-doped ZnO nanocrystals evidenced by positron annihilation spectroscopy, J. Appl. Phys., 112, 083905.

How to cite this article: Mohsen, M., El Okr, M.M., Gomaa, E., Hassan Ali, E., Essam, M., 2016. The effect of nickel doping on the structural, defect structural, optical and magnetic properties of zinc oxide nanoparticles. Scientific Journal of Review, 5(3), 360-370.